Thermal Response Characterization of an Environmental Test Chamber by means of Dynamic Thermal Models

Ali Saberi Derakhtenjani[1] , Andreas K. Athienitis[1] , José A. Candanedo[2], Vahid R.Dehkordi[2]
[1]BCEE Department, Concordia University, Montreal, Canada
[2]CanmetENERGY-Varennes, Natural Resources Canada, Varennes, Canada

Abstract

This paper presents an experimental and numerical characterization of the thermal behavior of the Environmental Test Chamber at Concordia University. This characterization is performed using frequency domain techniques, based on the analysis of building transfer functions.

The frequency domain model was developed from the application of first-principle heat transfer equations, and then validated and calibrated with experimental data. This paper also presents a modified least-squares curve fitting method (based on an existing technique) used to obtain transfer functions from discrete frequency responses.

Data not readily available in the experiments and required for the development of the frequency domain model was calculated with a lumped parameter finite difference model (LPFD).

1 Introduction

Motivation

This paper presents a numerical and experimental characterization of the thermal response of the Environmental Test Chamber (EC) at Concordia University, based on thermal modeling approaches. By developing and applying dynamic thermal models, valuable information can be obtained, for example, on how fast or how slow the Environmental Chamber responds to certain loads. The purpose of this work is to develop a generalized methodology and provide supporting information for further experiments and studies on control strategies in this unique test facility.

The EC, along with the Solar Simulator, allows testing and calibrating passive and active systems for buildings under diverse simulated weather conditions (e.g., outdoor temperatures of -40 °C to +50 °C). For example, a test hut with different advanced building technologies can be put inside the Environmental Chamber, thus enabling the study of its thermal response. Therefore, understanding the thermal behavior and response of the EC itself is important.

The interaction between a building and its HVAC system includes radiative and convective heat transfer as well as transient heat conduction. Conduction heat transfer is the cause for time delays in the building thermal response. From the thermal dynamics point of view, there are generally two types of elements and components in a building; the ones with high thermal capacities that have long-term dynamics (in the scale of hours) and the ones with small or negligible thermal capacitances that have short-term dynamics (in the scale of minutes). In order to investigate and study all the aspects of a building dynamics, the interaction between elements with both short-term and long-term dynamics should be taken into consideration

(Athienitis et al., 1990). A model meeting these requirements can be used more efficiently in control studies to improve the whole building energy management.

Modeling

Creating a model is the first and fundamental step in building energy management as it is the key tool to understand the system under study. Every model is created for one or more objectives, which may be to improve occupant comfort, to reduce energy consumption or to minimize operation costs.

Generally, a model consists of a structure that takes known information (inputs) and calculates desired information (outputs). The model structure can be created in many different ways. It may be a detailed, high-order model; or it may be a simple, low-order model optimized for a specific objective.

Creating a model of a system, selecting its type and its level of resolution is as much an art as it is a science. The inputs for a model are either controllable or non-controllable items. For example, in the context of the Environmental Chamber, the auxiliary heating and cooling supply is a controllable input which is being adjusted by a PID controller. In the case of buildings, non-controllable inputs (which are often called "disturbances") are mostly related to weather conditions (like solar radiation) and occupancy patterns.

Description of the Solar Simulator / Environmental Chamber Laboratory (PSE, 2009)

The Solar Simulator-Environmental Chamber (SSEC) laboratory is an experimental facility located at Concordia University in downtown Montreal, Canada. This facility allows accurate and repeatable testing of solar systems and advanced building envelopes under standard test conditions with well-simulated solar radiation and indoor plus outdoor conditions. It consists of two major systems:

1. A large scale Solar Simulator (Figure 1a) that is designed to emulate solar radiation in order to test solar systems such as photovoltaic modules, photovoltaic/thermal modules, solar air collectors, solar water collectors and a range of building-integrated solar systems. It consists of 8 metal halide lamps with an artificial sky to remove infrared radiation from lamps. It meets the specification of the standards EN 12975:2006 and ISO 9806-1:1994. The test specimen size can be up to 2.4 m × 3.2 m.
2. A two-storey high Environmental Chamber (EC) with a mobile solar simulator (Figure 1b) that is used to test building technologies under controlled environmental conditions, by simulating exterior/interior climates (from arctic to desert). This environmental chamber is the focus of the present paper. This facility has the following features:
    - Testing building envelope components, such as advanced wall systems that may include solar energy utilization components, under a range of conditions from Arctic to desert.
    - Developing test methods and design standards for predictable, relative hygrothermal performance and durability of different building envelope systems under various climatic conditions.
    - Testing wall systems and rooms up to 7 m high, for hygrothermal and energy performance, including solar electricity and useful heat generation.
    - Thermal control studies to improve building operation and reduce peak demand such as model predictive control. The temperature test range is -40°C to 50°C.

Figure 2 shows a schematic for the environmental chamber with a test room inside and mobile solar simulator:

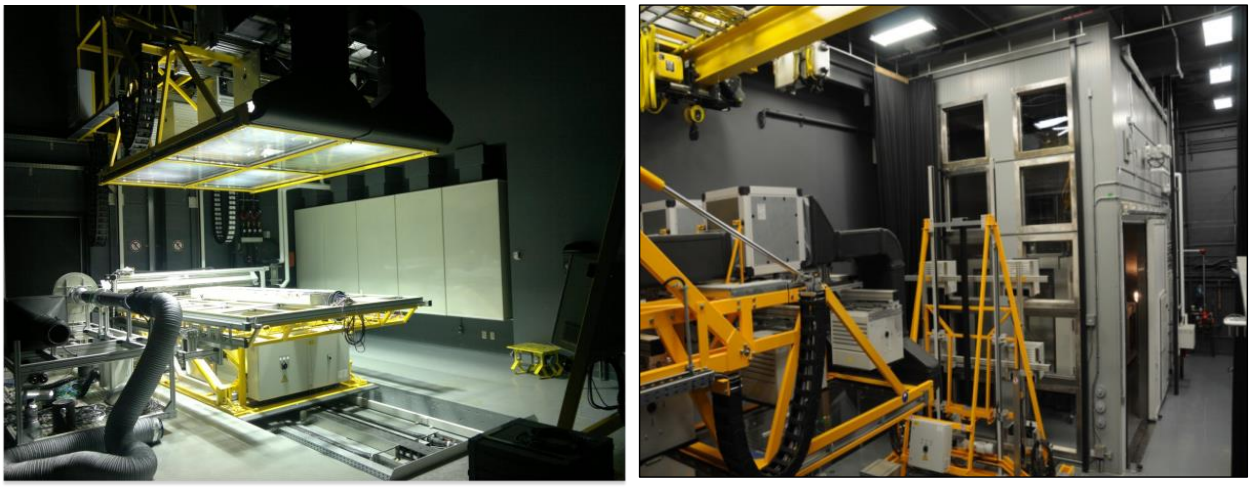

(a) (b)

Figure 1 .(a) Solar Simulator; (b) Environmental Chamber

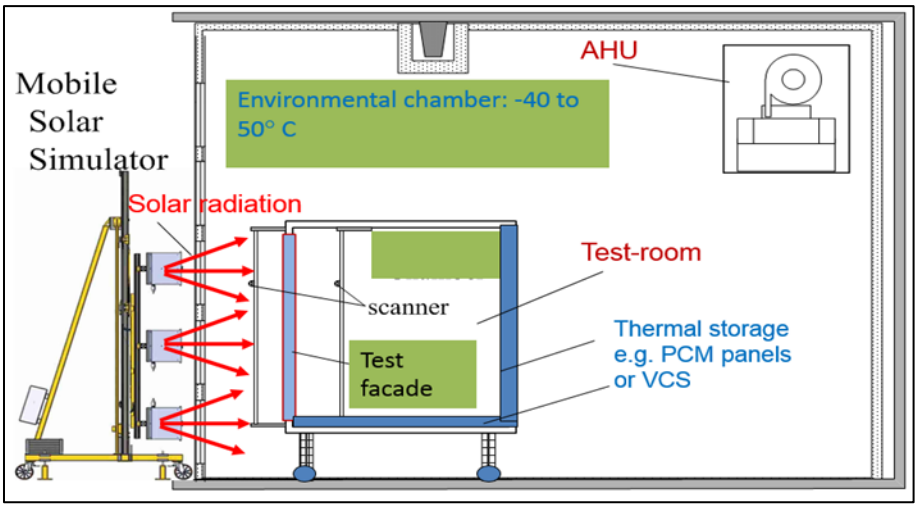

Figure 2. Schematic of environmental chamber with mobile solar simulator.

2 METHODOLOGY

The methodology presented here is primarily based on frequency domain modeling and determination of *s*-domain Laplace transfer functions for the environmental chamber. Frequency domain modeling provides a convenient method for analysis of periodic phenomena in which the main parameters of interest are the magnitude and phase angle of the room temperature and heat flows transfer functions (Athienitis and Santamouris, 2002). These transfer functions are informative and give important information about the thermal aspects and dynamics of the building. A key motivation for using a frequency domain model is that the majority of tests will require repeated simulated weather patterns (periodic). By using *s*-domain Laplace transforms, the exact solution can be obtained for the one-dimensional heat conduction differential equation (Athienitis and Santamouris, 2002).

A drawback of the frequency domain method is that it cannot accommodate nonlinearities. While a Lumped Parameter Finite Difference method (LPFD) can deal with non-linearities, conducting media with significant thermal mass must be discretized into a number of finite volumes modeled by lumped parameters; the discretization involves a loss of accuracy. In practice, assuming linearity in building elements has been shown to be a reasonable assumption.

Experiment description

To calibrate the model created for the chamber, an experiment has been set up. The Environmental Chamber has the following dimensions 8.9 m × 4.4 m × 7.12 m, corresponding to floor area of about 39.16 m^2, as shown in Figure 3a. The window area for the chamber is about 10 m^2 which consists of 10 double-glazing windows with the U-value of 2.9 W/(m^2°C). The floor is made of 15-cm (6-in) thick concrete which is the main thermal mass in the chamber. Polyisocyanurate insulation is installed between the interior surfaces and the exterior siding of the walls and ceiling. The walls and ceiling have the U-value of 0.19 W/(m^2°C). The air handling unit (AHU) providing cooling or heating is shown in Figure 3b. Sensors were attached to the interior surfaces of the chamber to measure the temperature of each surface. Additional sensors were used to measure the air temperature distribution inside the chamber. These sensors were shielded so that their temperature would not be affected directly by the solar radiation coming from the mobile solar simulator. The temperature variation inside the environmental chamber was programmed to be cyclic with a period of 1 cycle per day.

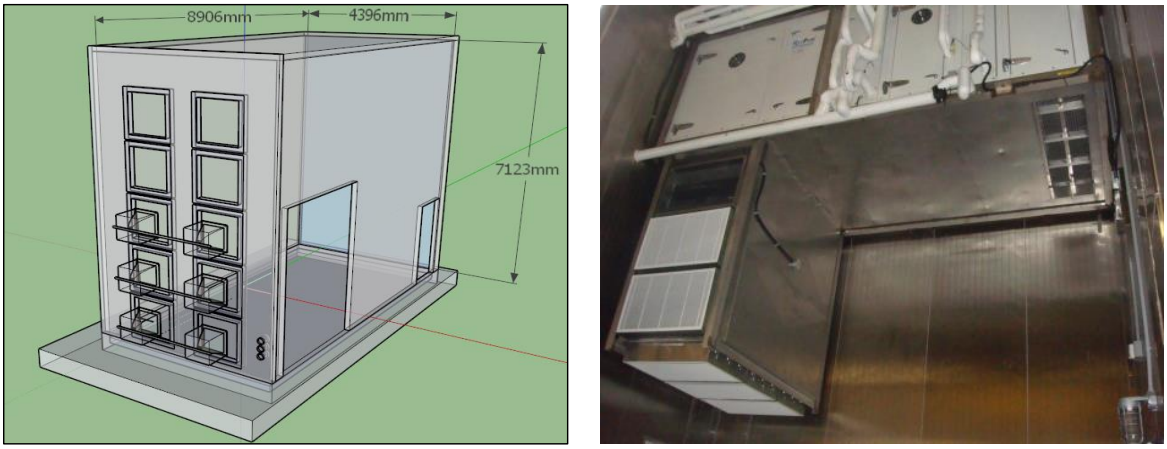

(a) (b)

Figure 3. (a) Schematic of environmental chamber (drawing by Jiwu Rao) (b) air handling unit (AHU)

Lumped Parameter Finite Difference Method (LPFD)

The auxiliary cooling/heating for the environmental chamber is supplied by the AHU with a programmable PID controller. Thus, a significant input in this case is the auxiliary heating or cooling supplied by the AHU. Auxiliary cooling/heating can be calculated from the supply and return temperatures and the air flow rate through the AHU. In this case, no sensor measuring the return temperature was available (but this can be estimated as the average temperature of the air in the chamber, which is measured). Also, the exact flowrate of the AHU was not available (new

sensors are being installed for this purpose) but local airflow measurements around the AHU were performed. A Lumped Parameter Finite Difference (LPFD) model was used to estimate the cooling/heating input and to study the detailed thermal dynamics of the space. An explicit finite difference method was used which is suitable for study of complex control strategies and nonlinear processes. A detailed lumped parameter finite difference model for environmental chamber has been created by using the thermal network shown in Figure 4:

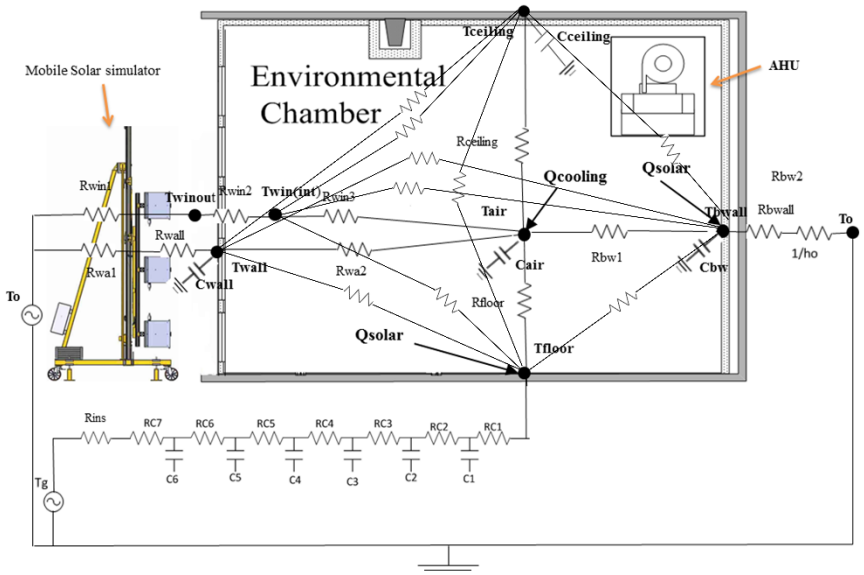

Figure 4 .Thermal network for finite difference method

In the above thermal circuit (Figure 4) the convective resistances connect each surface to the air node and radiative resistances interconnect interior surfaces. The following equations (1) and (2), derived by using the fully explicit finite difference scheme, are general forms of the finite difference formulation corresponding to node *i* at time interval *p* for the nodes with and without thermal capacitance respectively:

$$T_{i,p+1} = T_{i,p} + \frac{\Delta t}{C_i}\left(Q_i + \sum_j \frac{T_{j,p} - T_{i,p}}{R_{i,j}} \right) \tag{1}$$

$$T_{i,p+1} = \frac{Q_i + \sum_j \frac{T_{j,p}}{R_{i,j}}}{\sum_j \frac{1}{R_{i,j}}} \tag{2}$$

The auxiliary cooling load, Q_{aux}, was calculated at each time step by applying proportional control as in equation (3):

$$Q_{aux} = K_p \left(T_{setpoint} - T_{air} \right) \tag{3}$$

K_p is assumed to have the same value as the one in the existing controller for the Environmental Chamber, which is 6000 W/K. $T_{setpoint}$ is the desired temperature for the air that in this case defined as:

$$T_{\text{setpoint}} = 7.5\cos(\omega t) - 17.5 \quad [°\text{C}] \tag{4}$$

The solar irradiance from the mobile solar simulator is 1000 W/m^2 (on average). Then considering window area equal to 6 m^2 and glass transmittance of 93%, the solar heat gain in the chamber has the following profile shown in Figure 5:

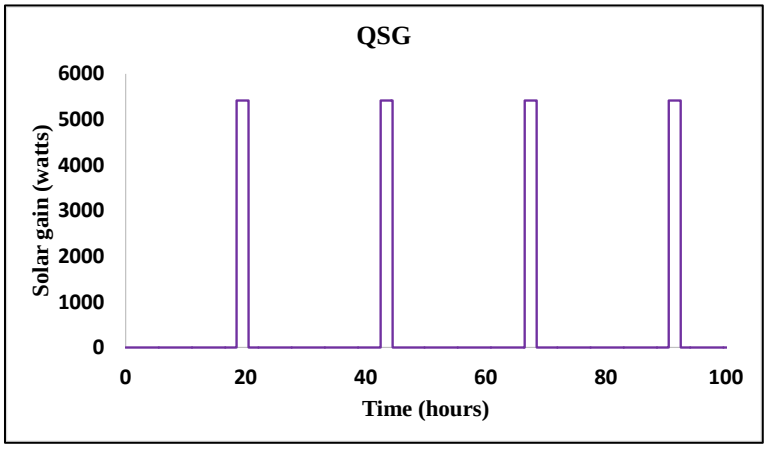

Figure 5. solar gain profile

The energy balance equations for all the nodes and the auxiliary cooling were solved simultaneously considering a time step of 30 seconds. The auxiliary cooling, calculated by the finite difference model (for the setpoint defined) is shown in Figure 6. The graph shows that the mean value for cooling is about 6 kW.

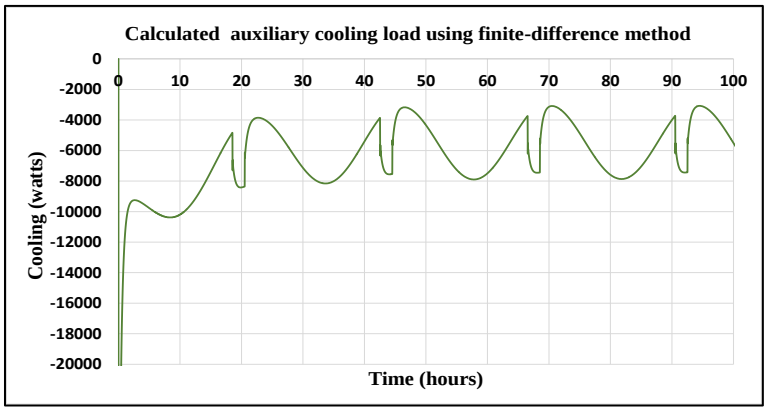

Figure 6. Cooling load profile calculated by LPFD model

Frequency domain model

Figure 7 shows the thermal network for the frequency domain model. The floor and each of the walls are represented by their Norton equivalent that consists of an equivalent heat source, Q_{eq}, and a self-admittance, Y_{self}. This representation eliminates all exterior nodes without needing to discretize the massive elements. The equivalent source is equal to the wall transfer admittance, Y_{transfer}, times an external specified temperature, T_{eq}, such as outdoor or sol-air temperature.

The admittances are calculated by using the following equations obtained from the cascade form of the wall heat conduction equations (Kimura, 1977):

$$Y_{\text{self},i} = \frac{U_i + A_i k_i \gamma_i \tanh(\gamma_i l_i)}{\frac{U_i}{A_i k_i \gamma_i}\tanh(\gamma_i l_i) + 1} \qquad Y_{\text{transfer},i} = \frac{-A_i}{\frac{A_i}{U_i}\cosh(\gamma_i l_i) + \frac{\sinh(\gamma_i l_i)}{k_i \gamma_i}}$$

where

$$\gamma_i = \sqrt{s/\alpha_i}, \qquad S = j\omega, \qquad j = \sqrt{-1}, \qquad \omega_n = \frac{2\pi \mathrm{n}}{24hrs}$$

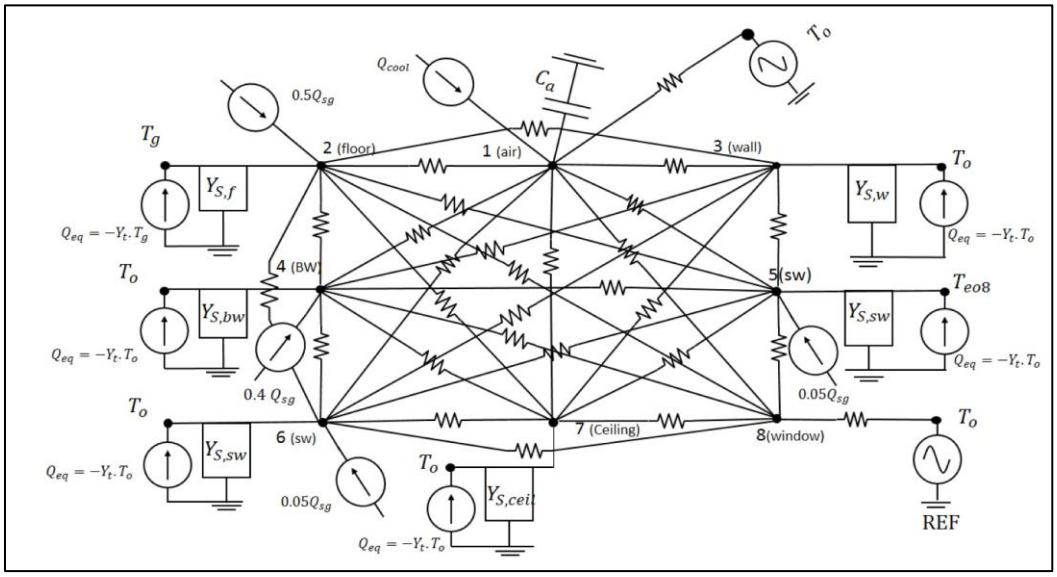

Figure 7. Thermal network for frequency domain model. Nodes: 1:air, 2:floor, 3:wall, 4:backwall, 5:sidewall, 6:sidewall, 7:ceiling, 8:window.

In Figure 7 the convective conductances, $U_{i1} = A_i h_{ci}$,connect the air node to the interior surfaces. The radiative conductances that interconnect the interior surfaces are given by, $U_{ij} = A_i F_{ij}^* \left(4\sigma T_m^3\right)$,where σ is the Stefan-Boltzman constant, $4T_m^3$ is the linearization factor and F_{ij}^* is the radiative exchange factor between surfaces *i* and *j* (Edwards, 1981). Writing the energy balance equation for the frequency domain thermal network yields:

$$\mathbf{YT = Q} \tag{5}$$

where **Y** is the admittance matrix, **Q** is the source matrix in which each element is the sum of the real and equivalent heat sources connected to a node. For example:

$$Q_1 = Q_{\text{cool}} + U_0 T_0, \text{ where } U_0 = U_{inf} + U_{win}, \qquad \text{for node 1}$$
$$Q_3 = -Y_{\text{transfer},3} \times T_0, \qquad \text{for node 3}$$

By expanding (5) we obtain:

$$\begin{bmatrix} sC_a + \sum_j U_{1j} + U_{\inf} & -U_{12} & -U_{13} & -U_{14} & -U_{15} & -U_{16} & -U_{17} & -U_{18} \\ -U_{12} & Y_{\text{Self},2} + \sum_j U_{2j} & -U_{23} & -U_{24} & -U_{25} & -U_{26} & -U_{27} & -U_{28} \\ -U_{13} & -U_{23} & Y_{\text{Self},3} + \sum_j U_{3j} & -U_{34} & -U_{35} & -U_{36} & -U_{37} & -U_{38} \\ -U_{14} & -U_{24} & -U_{34} & Y_{\text{Self},4} + \sum_j U_{4j} & -U_{45} & -U_{46} & -U_{47} & -U_{48} \\ -U_{15} & -U_{25} & -U_{35} & -U_{45} & Y_{\text{Self},5} + \sum_j U_{5j} & -U_{56} & -U_{57} & -U_{58} \\ -U_{16} & -U_{26} & -U_{36} & -U_{46} & -U_{56} & Y_{\text{Self},6} + \sum_j U_{6j} & -U_{67} & -U_{68} \\ -U_{17} & -U_{27} & -U_{37} & -U_{47} & -U_{57} & -U_{67} & Y_{\text{Self},7} + \sum_j U_{7j} & -U_{78} \\ -U_{18} & -U_{28} & -U_{38} & -U_{48} & -U_{58} & -U_{68} & -U_{78} & \sum_j U_{8j} \end{bmatrix} \begin{bmatrix} T_1 \\ T_2 \\ T_3 \\ T_4 \\ T_5 \\ T_6 \\ T_7 \\ T_8 \end{bmatrix} = \begin{bmatrix} Q_1 \\ Q_2 \\ Q_3 \\ Q_4 \\ Q_5 \\ Q_6 \\ Q_7 \\ Q_8 \end{bmatrix}$$

The elements of the admittance matrix can be written by inspection (Vlach and Singhal, 1983). The transfer functions are the elements of impedance matrix, $\mathbf{Z}=\mathbf{Y}^{-1}$, calculated at discrete frequencies. Thus the temperatures of the nodes are obtained by: $\mathbf{T}_i = \sum_{j=1}^{8} \left[\mathbf{Z}_{i,j} \mathbf{Q}_j \right]$

Obtaining Laplace transfer functions from discrete frequency responses

There are several methods to determine a continuous *s*-domain, Laplace transfer function from discrete frequency responses using different system identification techniques. One of the analytical methods consists of performing a least-squares complex interpolation on the discrete responses (Levy, 1959).

Assuming we have the values of $Z(j\omega)$ at discrete frequencies, the preferred form of the fitted polynomial may be expressed as:

$$Z_f(j\omega) = \frac{A_0 + A_1(j\omega) + A_2(j\omega)^2 + A_3(j\omega)^3 + \ldots}{B_0 + B_1(j\omega) + B_2(j\omega)^2 + B_3(j\omega)^3 + \ldots} \tag{6}$$

By separating the numerator and denominator into real and imaginary parts, equation (6) can be written as:

$$Z_f(j\omega) = \frac{\varepsilon + j\omega\beta}{\delta + j\omega\tau} = \frac{N(\omega)}{D(\omega)} \tag{7}$$

where:

$$\varepsilon = A_0 - A_2(j\omega)^2 + A_4(j\omega)^4 - \ldots \qquad \beta = A_1 - A_3(j\omega)^2 + A_5(j\omega)^4 - \ldots$$

$$\delta = 1 - B_2(\omega)^2 + B_4(\omega)^4 - \ldots \qquad \tau = B_1 - B_3(\omega)^3 + B_5(\omega)^4 - \ldots$$

Then we define the fit error as:

$$\zeta(\omega) = \left| Z(j\omega) - Z_f(j\omega) \right| = \left| Z(j\omega) - \frac{N(\omega)}{D(\omega)} \right| ,$$

Now, multiplying both sides by $D(\omega)$ we have:

$$D(\omega)\zeta(\omega) = D(\omega)Z(j\omega) - N(\omega) = a(\omega) + jb(\omega)$$

where $a(\omega)$ and $b(\omega)$ are functions of both frequency and the unknown coefficients A_i and B_i. Then we will have at any specific frequency:

$$|D(\omega)\zeta(\omega)|^2 = a^2(\omega) + b^2(\omega)$$

Now, defining E as the function that equals $a^2(\omega) + b^2(\omega)$ summed over all m frequencies as:

$$E = \sum_{n=0}^{m}\left[\left(r_n\delta_n - \omega_n\tau_n I_n - \varepsilon_n\right)^2 + \left(\omega_n\tau_n r_n + \delta_n I_n - \omega_n\beta_n\right)^2\right] \tag{8}$$

where:

$$r_n = \left(\text{Measured magnitude at } \omega_n\right) \times \cos\left(\text{measured phase angle at } \omega_n\right)$$

$$I_n = \left(\text{Measured magnitude at } \omega_n\right) \times \sin\left(\text{measured phase angle at } \omega_n\right)$$

Now the error function E will be minimized with respect to A_i and B_i, that is:

$$\frac{\partial E}{\partial A_i} = 0, \text{ and } \frac{\partial E}{\partial B_i} = 0,$$

which yields:

$$\begin{aligned}
\frac{\partial E}{\partial A_0} &= \sum_{n=0}^{m} -2(\delta_n r_n - \omega_n\tau_n I_n - \dot{o}_n) = 0 \\
\frac{\partial E}{\partial A_1} &= \sum_{n=0}^{m} -2\omega_n(\omega_n\tau_n r_n + \delta_n I_n - \omega_n\beta_n) = 0 \\
\frac{\partial E}{\partial A_2} &= \sum_{n=0}^{m} 2\omega_n^2(\delta_n r_n - \omega_n\tau_n I_n - \dot{o}_n) = 0
\end{aligned} \tag{8}$$

,…… and so on

It is assumed that $B_0 = 1$, now for B_i:

$$\begin{aligned}
\frac{\partial E}{\partial B_1} &= \sum_{n=0}^{m} -2\omega_n I_n(\delta_n r_n - \omega_n\tau_n I_n - \varepsilon_n) + 2\omega_n r_n\left(\omega_n\tau_n r_n + \delta_n I_n - \omega_n\beta_n\right) = 0 \\
\frac{\partial E}{\partial B_2} &= \sum_{n=0}^{m} -2\omega_n^2 r_n(\delta_n r_n - \omega_n\tau_n I_n - \varepsilon_n) - 2\omega_n^2 I_n\left(\omega_n\tau_n r_n + \delta_n I_n - \omega_n\beta_n\right) = 0 \\
\frac{\partial E}{\partial B_3} &= \sum_{n=0}^{m} 2\omega_n^3 I_n(\delta_n r_n - \omega_n\tau_n I_n - \varepsilon_n) - 2\omega_n^3 r_n\left(\omega_n\tau_n r_n + \delta_n I_n - \omega_n\beta_n\right) = 0
\end{aligned} \tag{9}$$

,……. and so on

Modification for a known steady state transfer function value (effective thermal resistance)

The steady-state response of a given input if often known. The Levy method was modified for the present problem as described below.

Let the variables λ, S, T, U be:

$$\lambda_h = \sum_{n=0}^{m} \omega_n^h, \quad S_h = \sum_{n=0}^{m} \omega_n^h r_n, \quad T_h = \sum_{n=0}^{m} \omega_n^h I_n, \quad U_h = \sum_{n=0}^{m} \omega_n^h \left(r_n^2 + \omega_n^2\right)$$

where the parameter h depends on the desired order of the transfer function. Because the steady state value of Z is already known (effective thermal resistance), then A_0 does not need to be evaluated. Thus,

$$A_0 = Z(\omega = 0) \quad \text{then} \quad \frac{\partial E}{\partial A_0} = 0 \ .$$

Now by rewriting and modifying the equations (9) and (10), the equations above can be written as 3 matrices, **M**, **N** and ***C***, for which their dimensions depend on the order of the transfer function we choose. Matrix **N** is the one that has the polynomial coefficients $(A_0, A_1, \ldots, B_0, B_1, \ldots)$. For example, for the 3rd order transfer function fitting, they will be:

$$\mathbf{M} = \begin{bmatrix} \lambda_2 & 0 & -\lambda_4 & -S_2 & T_2 & S_4 \\ 0 & -\lambda_4 & 0 & T_3 & S_4 & -T_5 \\ \lambda_4 & 0 & -\lambda_2 & -S_4 & T_5 & S_6 \\ -S_2 & -T_3 & S_4 & U_2 & 0 & -U_4 \\ T_3 & -S_4 & -T_5 & 0 & U_4 & 0 \\ -S_4 & -T_5 & S_6 & U_4 & 0 & -U_6 \end{bmatrix}, \mathbf{C} = \begin{bmatrix} T_1 \\ S_2 - A_0\lambda_2 \\ T_3 \\ -A_0 T_1 \\ U_2 - A_0 S_2 \\ -A_0 T_3 \end{bmatrix}, \qquad \mathbf{N = M^{-1}C}$$

For higher orders fits, the elements of matrices **M** and **C** can be obtained and modified by inspection. As an example, for the present case of the environmental chamber a third order transfer function for $Z_{1,1}$ (between room air temperature and sources entering to that node) has been obtained as:

$$Z_{1,1}(s) = \frac{0.005498 + (85.39)s + \left(9.078\times10^4\right)s^2 + \left(1.467\times10^7\right)s^3}{1 + \left(3.883\times10^4\right)s + \left(2.133\times10^8\right)s^2 + \left(8.216\times10^{10}\right)s^3} \tag{10}$$

The fitting error is typically less than 1%, except at one point which was around 1.7%.

3 Results

Model validation and calibration

The developed frequency domain model was calibrated by performing an experiment (Figure 8). In the calibration process it was observed that thermal bridges (openings for pipes, door frames, etc.) which exist in the chamber envelope have a significant effect and should be considered in the model. There is also a small heating system around the door frame in order to prevent the door from getting frozen and stuck on its frame when there is low-temperature inside.

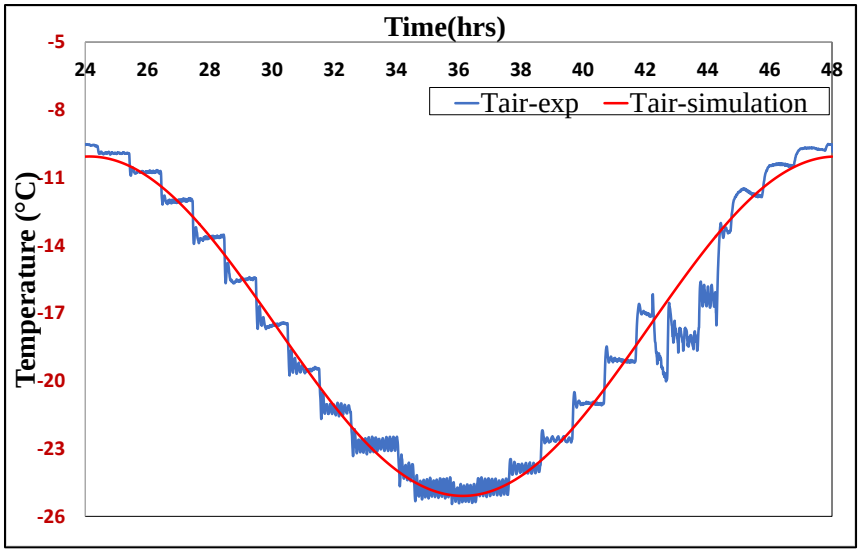

Figure 8. Air temperature profile; simulated vs. experimental

Frequency response and transfer function analysis

Thermal characteristics of a zone can be studied by analyzing its transfer functions. An important advantage of frequency domain modeling is that transfer functions can be easily obtained and studied. Let us consider $Z_{1,1}$,the transfer function between air temperature (T_1) and the "equivalent" heat source into node 1 (Q_1). Figure 9 shows the Bode plot for $Z_{1,1}$.

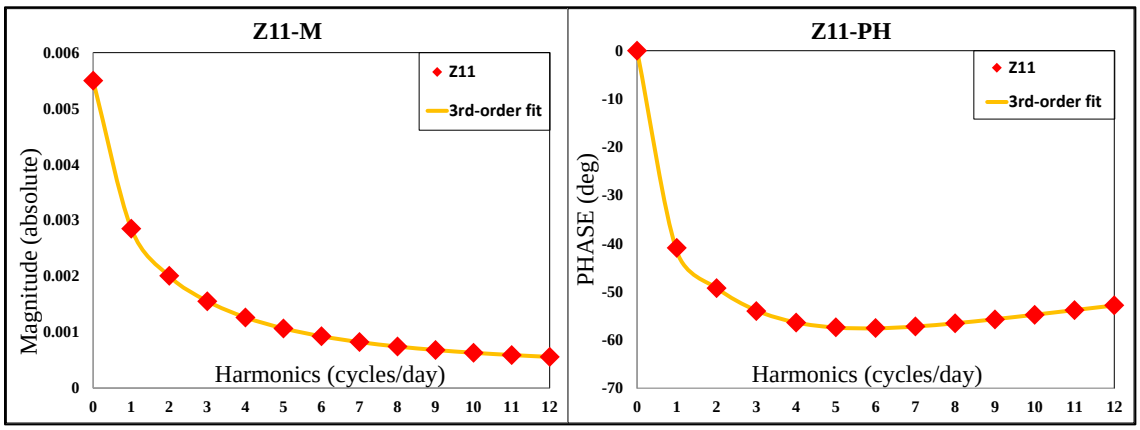

Figure 9.Bode plot for Z11

In the above plot for the *x*-axis, instead of frequency, ω_n, the harmonics, *n*, were used for easier interpretation. As can be seen from Figure 9, by increasing the frequency (cycles per day) the magnitude drops. This phenomenon corresponds to a typical low-pass filter effect: low-frequency signals "pass" while higher frequency signals are attenuated. It is important to consider that in the analysis of variables with a dominant diurnal harmonic (*n*=1) such as solar radiation and exterior temperature, the magnitude and phase of diurnal frequency is the most important to be studied (Athienitis and Santamouris, 2002). Thus, the most important harmonic is the 1 cycle/day which has the highest magnitude. One can determine the approximate delay in the response of the room temperature to Q_1, the auxiliary cooling load, by observing the phase

angle of the 1st harmonic. As shown in Figure 9, $\phi(\omega_1) = -40.89°$. The minus sign indicates a delay. From the above discussion this angle corresponds to a delay of:

$$40.89°\left(\frac{24\text{ h}}{360°}\right) \approx 2.72\text{ h}$$

in the room temperature response, T_1, to the source Q_1. This result is confirmed by looking at the time domain response (Figure 10):

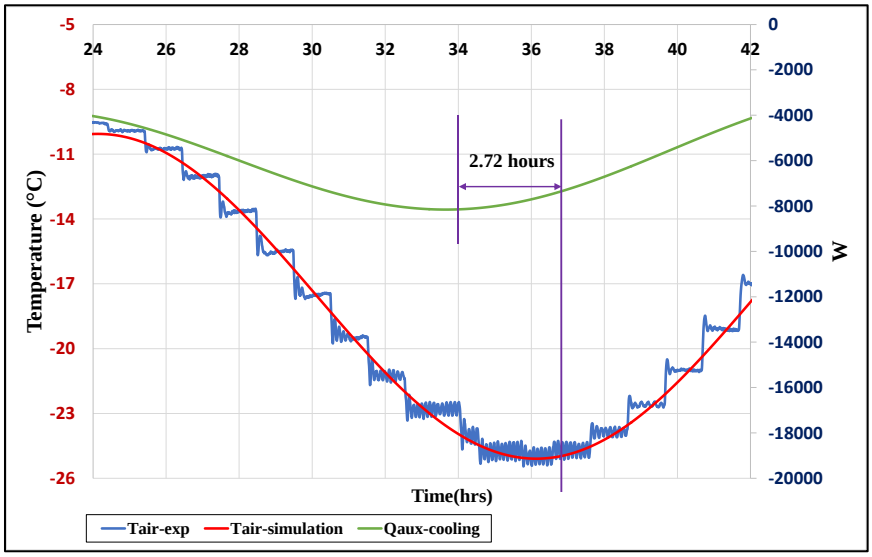

Figure 10. Delay in room temperature response

Another important transfer function is $Z_{1,2}$, between the solar radiation absorbed on the floor (node 2) and air temperature (node 1) in the zone. By examining its Bode plot, the delay in the response of the room temperature to the source Q_2 can be found. In this case the phase angle is -61.2°, indicating a delay of 4.08 hours in the room air temperature response to the solar gain on the floor. This is expected, because the concrete floor has a high thermal capacity and it takes a while for it to release the absorbed heat.

It is also important to study the thermal characteristics of the floor as it is the largest thermal mass in the chamber. The delay in the floor temperature (T_2) response to Q_1 (cooling load) and Q_2 (absorbed solar radiation on the floor) is 4.079 h and 2.86 h respectively. This information is extremely important for designing control strategies for the environmental chamber for different tests.

4 Conclusions

Contributions

This paper has presented a methodology for thermal response characterization of the EC at Concordia University by means of thermal models. The main contributions of this paper are: (a) the utilization of frequency domain techniques, along with experimental data, for the characterization of the EC; (b) the derivation of a modified least squares curve fitting technique for building transfer functions with a known steady-state response.

First, a lumped parameter finite difference (LPFD) model was created. The auxiliary cooling was calculated by implementing a proportional control strategy in the LPFD model (Figure 4). Then, a detailed frequency model, based on a methodology by Athienitis et al. (1990) was developed. In this model, the walls and other surfaces with thermal mass are represented by a two-port network (Norton equivalent) consisting of a surface self-admittance and an equivalent heat source. Figure 7 shows the thermal circuit for this model. The transfer functions of interest are the elements of impedance matrix, $\mathbf{Z} = \mathbf{Y}^{-1}$, obtained at discrete frequencies.

An analytical modified least square complex curve fitting technique was derived and presented to obtain a mathematical equation for building transfer functions (based on the method by Levy, 1959). It was shown that a third order transfer function fits well with the discrete frequency responses.

Transfer functions obtained from the frequency domain model were studied and important thermal characteristics of the zone, such as the delay in the temperature response to a specific heat source were observed.

Final comments

Despite its limitations, a study of frequency domain response has several advantages: (a) it can be used for either simulation or analysis, while no analysis can be made in time domain without a simulation; (b) computational efficiency; (c) exact heat conduction solutions (no need for thermal mass discretization); (d) leveraging the superposition principle to analyze the impact of different sources (e.g., examine the free-floating response by turning off the auxiliary source).

It is of course possible to create a model with an existing simulation tool, or to develop a highly detailed model. However, parsimony is important in control-oriented models, since the model needs to be ultimately calibrated with an existing building, and eventually used by an automatic controller. Too much information might add confusion and complicate the implementation without adding much benefit.

Further studies are needed on the application of the presented modeling methodology for the design of control strategies for buildings. The methodology can be extended for multi-zone buildings. In that case, it would be interesting to consider time-domain and frequency domain analyses of low-order, grey-box, equivalent RC circuits for complex buildings with many zones. Some recent studies by Candanedo et al. (2013) have shown that such a model can be accurate enough for the purpose of model predictive control (MPC) implementation for the buildings.

5 Acknowledgements

Financial and technical supports have been provided through NSERC/Hydro-Québec industrial research chair. In-kind and technical supports from CanmetENERGY were also provided. The authors would like to thank Dr. Jiwu Rao for his help during the progress of this work, in the setting up of the experiment and data acquisition and for his valuable comments on the results.

6 Nomenclature

A_i	Area for node *i*
α_i	Thermal diffusivity $k/(\rho c_p)$ of surface *i*
C_i	Thermal capacitance for node *i*
C_a	Thermal capacitance for the air node

i	Node number "i" (thermal models)/or "ith" coefficient (curve fitting section)
j	Imaginary $(-1)^{0.5}$ &/or Node number "j" in frequency domain model
k	Thermal conductivity
K_p	Proportional control gain , W/°C
n	Harmonic
p	Index and counter for time step
Q_{aux}	Auxiliary power input, W
Q_i	Source at node I, W
R	Thermal resistance, K/W
s	Laplace variable
$T_{i,p}$	Temperature of node i at p^{th} time step,
$U_{i,j}$	Radiative or convective conductance between nodes(or surfaces) i, j, W/K
U_{inf}	Infiltration U-value for the chamber
U_{win}	Total U-value of the Window
ω_n	Frequency at n^{th} harmonic
$Y_{self,i}$	self-admittance of surface(node) i
$Y_{transfer,i}$	transfer-admittance of surface(node) i
$\mathbf{Y}$	Admittance matrix
$Z_{i,j}$	Impedance transfer function between node i and j
$\mathbf{Z}$	Impedance matrix
Δt	Time step

7 References

Athienitis, A. 1994. *Building Thermal Anlysis, An Electronic Mathcad Book*.

Athienitis, A. & Santamouris, M. 2002. *Thermal Analysis and Design of Passive Solar Buildings,* London, UK, James & James.

Athienitis, A., Stylianou, M. & Shou, J. 1990. *A Methodology for Building thermal dynamics studies and control applications. ASHRAE Transactions*, 96.

Candanedo , A.J., Dehkordi , R.V. & Lopez , Ph. 2013. *A Control-oriented simplified building modeling strategy,* Chambery, France, *IBPSA Conference proceedings*.

Edwards, D. K. 1981. *Radiation heat transfer notes,* New York, Hemisphere.

Kimura, K. 1977. *Scientific basis for air-conditioning,* London, Applied Science Publishers Ltd.

Levy, E. C. 1959. Complex curve fitting. *IRE Transactions on Automatic Control***,** 37-43.

PSE 2009. *Indoor test stand & Solar Thermal collectors*. Freiburg, Germany.

Vlach, J. & Singhal, K. 1983. *Computer methods for circuit analysis and design,* New York, Van Nostrand Reinhold Co.